Modification of two-level-atom resonance fluorescence near a plasmonic nanostructure

Yulia V. Vladimirova,[1,*] Vasily V. Klimov,[2] Vladimir M. Pastukhov,[1] and Victor N. Zadkov[1]

[1]*International Laser Center and Faculty of Physics, M. V. Lomonosov Moscow State University, Moscow 119992, Russia*

[2]*P. N. Lebedev Physical Institute, Russian Academy of Sciences, Leninsky Avenue 53, 119991 Moscow, Russia*

(Received 9 February 2012; revised manuscript received 10 April 2012; published 7 May 2012)

Modification of the resonance fluorescence spectrum of a two-level atom driven by a monochromatic field in the close proximity of a plasmonic nanostructure (metal sphere) is studied in detail. It is shown that one can control this spectrum by varying several key parameters: (i) the radius of the nanosphere, (ii) polarization of the incident radiation, and (iii) the atom's location around the nanosphere (its radial coordinate and polar angle in the spherical coordinate system). These parameters affect the local field enhancement and the modification of the radiative decay rate of the atom interacting with the nanosphere, which leads to modification of the resonance fluorescence spectrum of the atom (e.g., frequency shift of the satellite lines in the Mollow-type triplet, widths of the lines, and the spectrum intensity) by contrast with that in free space. The permittivity of the metal the nanosphere is made of is also an additional parameter, which defines the nonradiative decay. The latter in combination with other parameters allows continuous control of the transition from resonance fluorescence enhancement to its quenching.

DOI: 10.1103/PhysRevA.85.053408 PACS number(s): 33.50.−j, 68.37.Uv, 73.20.Mf, 78.67.Bf

I. INTRODUCTION

Since the early indication by Sommerfeld [1] and then the pioneering work of Purcell [2] it is well known that the radiative properties of an emitter (specifically atom, molecule, or quantum dot) are strongly modified in confined geometries (for review, see also Refs. [3,4]). Moreover, when the quality factor of a nanoparticle, for instance, is high enough, the emitted photon can be absorbed and then reradiated by the particle. As a result, the exponential decay of the excited level is changed to vacuum Rabi oscillations [5–7].

Of special interest is the interaction of atoms and molecules with plasmonic nanostructures. It has been shown not only that plasmonic nanostructures work as optical antennas converting the incoming radiation to localized energy and vice versa, generating spots of significant enhancement of the local field, but also the lifetime of an excited quantum emitter state of the emitter located near the nanostructure is affected by the radiative decay rate due to photon emission and by the nonradiative decay rate due to energy dissipation in the environment. Both these rates for atoms and molecules close to metal surfaces can be enhanced [8–14]. This results in one of the important applications of nanoplasmonics—using plasmonic nanostructures for amplifying fluorescence [surface-enhanced fluorescence (SEF)] and Raman scattering [surface-enhanced Raman scattering (SERS)] [15–19]; and single-molecule sensitivity has been achieved experimentally [20–27].

Fluorescence studies also demonstrate that the fluorescence of a single quantum emitter in close proximity of a nanostructure results from both excitation of the emitter by the incident field, which is modified by the local environment, and emission of radiation that is modified by the balance of radiative and nonradiative decays [12,28–36]. This results in the continuous transition from fluorescence enhancement to fluorescence quenching while varying the distance between the emitter and the nanoparticle [27,37,38]. Most fluorescence studies of a single atom, molecule, or quantum dot have been done using spontaneous fluorescence, whereas the resonance fluorescence, which occurs when the quantum emitter is illuminated by an electromagnetic wave with frequency close to the emitter's resonant frequency, from emitter(s) in a confined geometry occurs just at the start [39,40]. The key advantage of the resonant fluorescence over the spontaneous one is that the resonance fluorescence exhibits much more information about the system under study, including quantum features of interaction of the incident radiation with the system [41].

By analogy with fluorescence, the resonance fluorescence of an atom near the plasmonic nanostructure must also be influenced by the modified incident electromagnetic field and by the modified radiative decay rate of the atom. Moreover, in the case of a strong incoming field, when the Rabi frequency is larger than the modified radiative decay rate, the spectrum of the resonance fluorescence of a two-level atom becomes more enriched and reveals three lines (see Sec. III), with positions and widths that bring new valuable information about the atom and the whole system under study [39]. It is important to note that the general theory of resonance fluorescence [41] can be readily applied for this case.

In this paper, we analyze theoretically the modification of the resonance fluorescence spectrum of a two-level atom driven by a monochromatic field near the plasmonic nanostructure, which we consider to be for simplicity a metallic nanosphere, as a function of the parameters of the nanosphere (its size and the permittivity), the polarization of the incident radiation, and the atom's location around the nanosphere. We have restricted ourselves to the two-level atom because we want to pay attention to the principal features of resonance fluorescence near a nanoparticle. However, our approach can be also generalized to multilevel atoms in a manner analogous to the method applied for multilevel atoms in free space [42–44].

The arrangement of the atom-nanosphere–incident field system is given in Fig. 1. A two-level atom with ground and excited states and with dipole moment **d** is placed in

*yu.vladimirova@physics.msu.ru

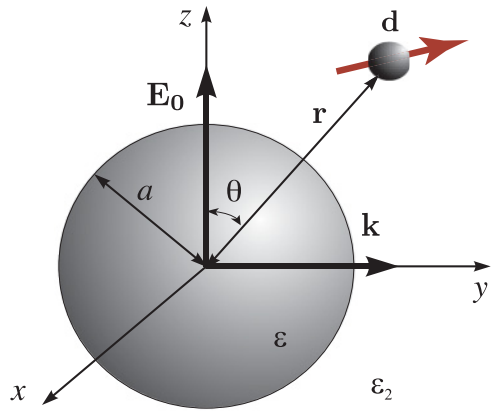

FIG. 1. (Color online) Arrangement of the problem.

close proximity to the metal nanosphere of radius a. The latter is located in the origin of the coordinate system. The atom's location around the nanosphere is defined by its radial coordinate $|\mathbf{r}|$ and the polar angle θ (in a spherical coordinate system); ε and ε_2 are the permittivities of the metal the nanosphere is made of and the space our atom-nanosphere system is placed in, respectively [45]. To be more specific, we assume that the nanosphere is made of silver; i.e., its permittivity is equal to $\varepsilon = -15.37 + i0.231$ and the wavelength of the incident laser field is $\lambda = 632.8$ nm. We also assume for simplicity that $\varepsilon_2 = 1$. The incoming z-polarized electromagnetic radiation $\mathbf{E}_0$ at the frequency ω_L, which is close to the frequency ω_0 of the atomic dipole transition from the ground to the excited state, has the wave vector $\mathbf{k}$ directed along the y axis. It is important to note also that the direction of the atomic dipole moment coincides with the direction of the local field created by the (atom-nanosphere–excited radiation) system in the point of space the atom is located [46].

The paper is organized as follows. In Sec. II we give an overview of the mechanisms of modification of the local field and radiative and nonradiative decay rates of the two-level atom located in close proximity to a metal nanosphere. Simple analytical expressions are given for both the local field enhancement and the modified total decay rate of the atom near the metal nanosphere. Section III is targeted at the calculation of the resonance fluorescence spectrum of the two-level atom near the metal nanosphere and it is shown that there are several parameters of the problem, which can be varied to control the spectrum. In conclusion, we summarize the received results and discuss some possible applications.

II. THE ATOM'S EXCITATION AND RADIATIVE AND NONRADIATIVE DECAY RATES NEAR THE PLASMONIC NANOSTRUCTURE

Electric field intensity in close proximity to the nanobody, which has size significantly less than the wavelength $\lambda = 632.8$ nm of the incoming field, can be calculated in the quasistatic approximation, which implies that no retardation effects are taken into account. For the nanosphere of radius $a = 20$ nm in the homogeneous incident electric field, only dipole resonances with $n = 1$ are excited and the field inside the nanosphere is equal to

$$\mathbf{E} = E_r\hat{\mathbf{n}}_r + E_\theta\hat{\mathbf{n}}_\theta = E_0\frac{3}{\varepsilon(\omega)+2}(\cos\theta\hat{\mathbf{n}}_r - \sin\theta\hat{\mathbf{n}}_\theta). \quad (1)$$

Outside the nanosphere, it becomes

$$\mathbf{E} = E_r\hat{\mathbf{n}}_r + E_\theta\hat{\mathbf{n}}_\theta = E_0(\cos\theta\hat{\mathbf{n}}_r - \sin\theta\hat{\mathbf{n}}_\theta) + E_0\frac{a^3}{r^3}\frac{\varepsilon(\omega)-1}{\varepsilon(\omega)+2}(2\cos\theta\hat{\mathbf{n}}_r + \sin\theta\hat{\mathbf{n}}_\theta), \quad (2)$$

where E_0 is the amplitude of the incident field, $\hat{\mathbf{n}}_r$, $\hat{\mathbf{n}}_\theta$ are the unit vectors in the spherical coordinate system, $\varepsilon(\omega)$ is the permittivity of the nanobody at the frequency ω. It is also worth noting here that in the case of a sphere $E_\phi = 0$.

Figure 2 shows the spatial distribution of radial and tangential components of $|\mathbf{E}|^2/|\mathbf{E}_0|^2$ in the vicinity of a silver nanosphere in the yz plane calculated by Eq. (2).

In the external electromagnetic field, the dipole moment of the atom is directed along the direction of the field in the point of space where the atom is located. From Fig. 3, which shows the distribution of the local field vectors in the vicinity of the nanosphere, one can clearly see that the direction of the local field and its intensity essentially depend on $\mathbf{r}$, so the Rabi

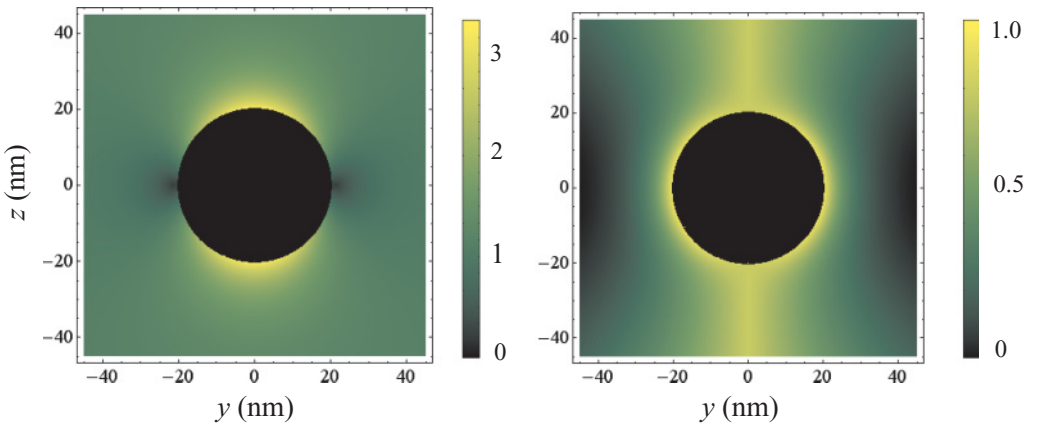

FIG. 2. (Color online) Spatial distribution of radial E_r (left) and tangential E_θ (right) field components in the vicinity of a silver nanosphere in the yz plane, calculated by Eq. (2). The sphere radius is $a = 20$ nm, $\lambda = 632.8$ nm, and the incident field is polarized along the z axis.

frequency Ω also depends on $\mathbf{r}$ and can be written as

$$\Omega(\mathbf{r}) = \frac{d}{\hbar}\sqrt{|E_r|^2 + |E_\theta|^2 + |E_\varphi|^2}. \tag{3}$$

With the help of Eq. (2), Eq. (3) takes the form

$$\Omega(\mathbf{r}) = \frac{d}{\hbar}\sqrt{|E_r|^2 + |E_\theta|^2} = \frac{d}{\hbar}\sqrt{\left|E_0\cos\theta\left(\frac{2a^3}{r^3}\frac{\varepsilon(\omega)-1}{\varepsilon(\omega)+2}+1\right)\right|^2 + \left|E_0\sin\theta\left(\frac{a^3}{r^3}\frac{\varepsilon(\omega)-1}{\varepsilon(\omega)+2}-1\right)\right|^2}, \tag{4}$$

where the atomic dipole transition moment is equal (in the Gaussian system of units) to

$$d = \left(\frac{3\gamma_0\hbar c^3}{4\omega_0^3}\right)^{\frac{1}{2}}, \tag{5}$$

where ω_0 is the frequency of the atomic dipole transition and γ_0 is the radiative decay rate of the atom in free space [41].

The total normalized linewidth of the atom located at the point with radius vector $\mathbf{r}$ and with the atomic dipole moment directed along the direction of the local field in this point can be defined as (see Sec. 6.3 of Ref. [3])

$$\gamma/\gamma_0 = \{\cos^2\xi(\gamma/\gamma_0)_{\text{rad}} + \sin^2\xi(\gamma/\gamma_0)_{\text{tan}}\}, \tag{6}$$

where γ_{rad} is the total decay rate of the atom near the nanosphere for the radial orientation of the dipole moment toward the nanosphere and γ_{tan} is that for the tangential orientation; γ_0 is the natural linewidth of the atom in free space and ξ is the angle between the directions of the dipole moment and $\mathbf{r}$. Taking into account that

$$\cos^2\xi = \frac{|E_r|^2}{\sqrt{|E_r|^2 + |E_\theta|^2 + |E_\varphi|^2}},$$
$$\sin^2\xi = \frac{|E_\theta|^2 + |E_\varphi|^2}{\sqrt{|E_r|^2 + |E_\theta|^2 + |E_\varphi|^2}},$$

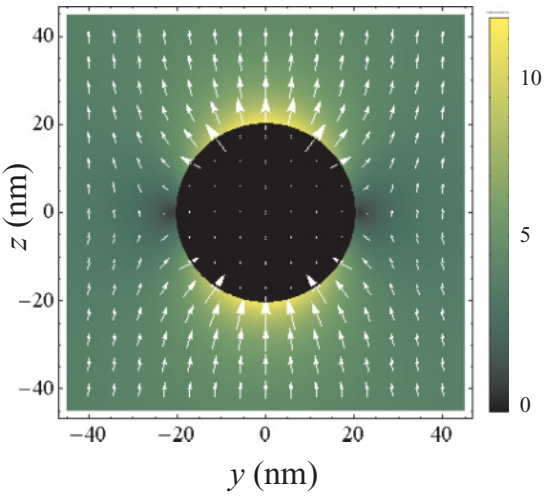

FIG. 3. (Color online) Distribution of the field **E** vectors mapped on the total density of the field in the vicinity of a silver nanosphere in the yz plane, calculated by Eq. (2). The sphere radius is $a = 20$ nm, $\lambda = 632.8$ nm, and the incident field is polarized along the z axis.

Eq. (6) can be rewritten in the form

$$\gamma/\gamma_0 = \frac{|E_r|^2(\gamma/\gamma_0)_{\text{rad}} + (|E_\theta|^2 + |E_\varphi|^2)(\gamma/\gamma_0)_{\text{tan}}}{\sqrt{|E_r|^2 + |E_\theta|^2 + |E_\varphi|^2}}, \tag{7}$$

where $(\gamma/\gamma_0)_{\text{rad}}$ is the total decay rate for the radial orientation of the atomic dipole moment that can be expressed as

$$\left(\frac{\gamma}{\gamma_0}\right)_{\text{rad}} \xrightarrow{|\mathbf{k}|a\to 0} \frac{3}{2(|\mathbf{k}||\mathbf{r}|)^3}\text{Im}\sum_{n=1}^{\infty}(n+1)^2\left(\frac{a}{|\mathbf{r}|}\right)^{2n+1}\frac{\alpha_n}{a^{2n+1}} + \left|1+\frac{2\alpha_1}{|\mathbf{r}|^3}\right|^2 + O\left(\frac{1}{|\mathbf{k}|a}\right) \tag{8}$$

and $(\gamma/\gamma_0)_{\text{tan}}$ is the total decay rate for the tangential orientation of the atomic dipole moment, which is equal to

$$\left(\frac{\gamma}{\gamma_0}\right)_{\text{tan}} \xrightarrow{|\mathbf{k}|a\to 0} \frac{3}{4(|\mathbf{k}||\mathbf{r}|)^3}\text{Im}\sum_{n=1}^{\infty}n(n+1)\left(\frac{a}{|\mathbf{r}|}\right)^{2n+1}\frac{\alpha_n}{a^{2n+1}} + \left|1-\frac{\alpha_1}{|\mathbf{r}|^3}\right|^2 + O\left(\frac{1}{|\mathbf{k}|a}\right), \tag{9}$$

where

$$\alpha_n = a^{2n+1}\frac{\varepsilon(\omega)-\varepsilon_2}{\varepsilon(\omega)+\varepsilon_2(n+1)/n} \tag{10}$$

are the multipole polarizabilities of nth order that generalize the dipole polarizability at $n = 1$.

The normalized decay rates $(\gamma/\gamma_0)_{\text{rad, tan}}$ near the nanosphere in the plane $x = 0$ are shown in Fig. 4, from which one can readily see that the normalized radiative decay rate for the atom with tangential orientation of the dipole moment goes to zero when the atom approaches the surface of the nanosphere. This is due to the fact that the dipole moment induced in the metal nanosphere is almost equal in amplitude to the atomic dipole moment, but oppositely directed. As a result, an atom with dipole moment orientation tangential to the nanosphere surface has a slow decay rate, whereas an atom with a normal orientation of the atomic dipole moment to the nanosphere surface has a rather high decay rate.

The first term in Eqs. (8) and (9) describes the nonradiative atomic decay rate, i.e., that part of the atom's energy which is converted to heat. The radiative decay rate of the atom is defined actually by the second term in Eqs. (8) and (9). For a sphere characterized by some losses, the total atomic decay rate includes a term that increases infinitely as $1/(|\mathrm{k}|a)^3$ with decreasing sphere radius. For the atom in very close proximity to the nanosphere, the series in Eqs. (8) and (9) are diverged; thus, for the sphere with losses the nonradiative decay rate

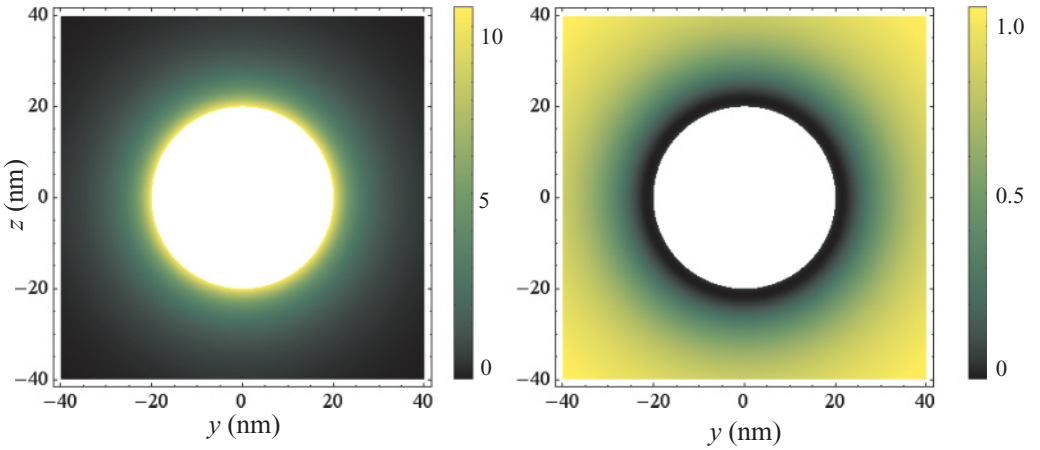

FIG. 4. (Color online) The normalized radiative decay rates $(\gamma/\gamma_0)_{\text{rad, tan}}$ near the nanosphere in the plane $x = 0$ for the radial (left) and tangential (right) atomic dipole moment orientations. The sphere radius is $a = 20$ nm, and $\varepsilon = -15.37 + i0.231$ at $\lambda = 632.8$ nm.

goes to infinity while the atom approaches the surface of the sphere. This leads to so-called fluorescence quenching, which is observed at distances of less than 5 nm between the atom and the nanosphere surface, when the nonradiative decay rate prevails over the radiative decay ones. Figure 5 shows (in logarithmic scale) how the radiative, nonradiative, and total decay rates correspond to each other for the silver nanosphere we use in our calculations.

With the help of Eqs. (8) and (9), taking into consideration both the radiative and nonradiative atomic decay rates in our calculations of the resonance fluorescence spectrum in the next section of the paper allows us to correctly analyze the spectrum variations versus the location of the atom even at the very small distances between the atom and the nanosphere.

As we have already mentioned, the resonance fluorescence spectrum depends on the Rabi frequency, i.e., the local field amplitude and the direction of this field, and the total decay rate, which are all affected by the presence of the nanoparticle. The atomic resonance near the plasmonic nanoparticle is also shifted at the frequency about the linewidth, so that to observe the resonance fluorescence one needs to adjust the incident laser frequency at the value of this frequency shift [35].

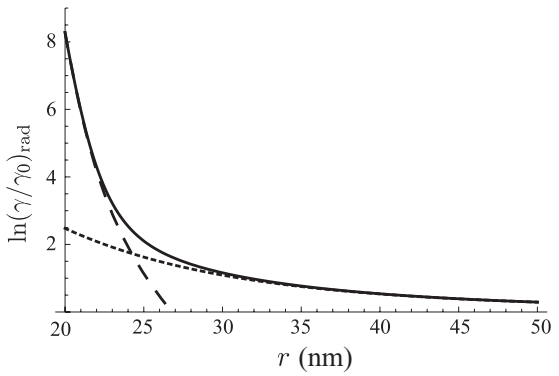

FIG. 5. Radial components of the radiative (dotted line), nonradiative (dashed line), and total (solid line) decay rates for the spherical silver particle of radius $a = 20$ nm, $|\mathrm{k}|a = 0.2$, and $\varepsilon = -15.37 + i0.231$ at $\lambda = 632.8$ nm.

III. CALCULATION OF THE RESONANCE FLUORESCENCE SPECTRUM

The spectrum of resonance fluorescence of a two-level atom in free space exhibits three well-separated spectral lines at sufficiently high intensity of the driving monochromatic field and coherent and homogeneously broadened incoherent lines for a weak excitation. This fluorescence triplet, which is sometimes referred to as a Mollow triplet, was predicted by Apanasevich [47,48] and then by Newstein [49] and Mollow [50] and has been observed and studied in detail experimentally (for details see Ref. [51]). Figure 6 shows the dressed-state energy-level structure of the singly dressed two-level atom (Fig. 6, left) and illustrates the formation of the resonance fluorescence spectrum (Fig. 6, right).

The theory of resonance fluorescence is well developed and the general approach presented in Ref. [41] can be readily applied to the case of an atom in any environment.

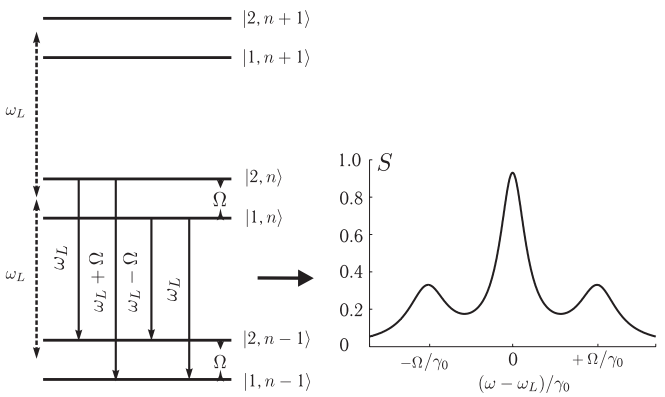

FIG. 6. The dressed-state energy-level structure of the singly dressed two-level atom (left), which consists of an infinite number of manifolds $[\ldots,(n-1),(n),(n+1),\ldots]$, each of which is composed of the doublet $|1,n\rangle$, $|2,n\rangle$ levels, where n is the mean number of photons in the mode ω_L. The interdoublet and intradoublet (in the limit of the strong field, $n \gg 1$) separations are ω_L and Ω, respectively. Transitions contributing to the spectra are shown in solid arrows and the resulting resonance fluorescence spectrum (right) consists of three lines.

From that theory it follows that the spectral density of the fluorescence emitted by a driven atom (resonance fluorescence) is defined by the normally ordered correlation function $\langle E^{(-)}(\mathbf{r},t)E^{(+)}(\mathbf{r},t+\tau)\rangle$ of the fluorescent light at some suitably chosen point $\mathbf{r}$ in the far field, where $E^{(+)}(\mathbf{r},t)$, $E^{(-)}(\mathbf{r},t)$ are the positive- and negative-frequency parts of the electric field operator:

$$S(\mathbf{r},\omega_L) = \mathrm{Re}\int_0^\infty d\tau \langle E^{(-)}(\mathbf{r},t)E^{(+)}(\mathbf{r},t+\tau)\rangle e^{i\omega_L\tau}. \quad (11)$$

For the two-level atom, the correlation function simplifies to

$$\begin{aligned}&\langle E^{(-)}(\mathbf{r},t)E^{(+)}(\mathbf{r},t+\tau)\rangle \\ &\quad = I_0(\mathbf{r})\sin^2\psi\, e^{-i\omega\tau}\left(\frac{\Omega^2(\mathbf{r})}{\gamma^2(\mathbf{r})+2\Omega^2(\mathbf{r})}\right) \\ &\qquad \times\left[\frac{\gamma^2(\mathbf{r})}{\gamma^2(\mathbf{r})+2\Omega^2(\mathbf{r})}+\frac{e^{-\gamma\tau/2}}{2}+\frac{e^{-3\gamma\tau/4}}{4}\right. \\ &\qquad \left.\times\{e^{-i\mu(\mathbf{r})\tau}[P(\mathbf{r})+iQ(\mathbf{r})]+e^{i\mu(\mathbf{r})\tau}[P(\mathbf{r})-iQ(\mathbf{r})]\}\right],\end{aligned} \quad (12)$$

where $I_0(\mathbf{r}) = [(\omega^2|\mathbf{d}|)/(c^2|\mathbf{r}|)]^2$, and ψ is the angle between the z axis and the direction of the dipole, which is located in the plane yz [41]. We assume that the observer is located at the z axis, and $P = P(\mathbf{r})$, $Q = Q(\mathbf{r})$, and $\mu = \mu(\mathbf{r})$ are defined as

$$\begin{aligned}&P(\mathbf{r}) = \frac{2\Omega^2(\mathbf{r})-\gamma^2(\mathbf{r})}{2\Omega^2(\mathbf{r})+\gamma^2(\mathbf{r})}, \quad Q(\mathbf{r}) = \frac{\gamma(\mathbf{r})}{4\mu(\mathbf{r})}\frac{10\Omega^2(\mathbf{r})-\gamma^2(\mathbf{r})}{2\Omega^2(\mathbf{r})+\gamma^2(\mathbf{r})}, \\ &\mu(\mathbf{r}) = \left(\Omega^2(\mathbf{r})-\frac{\gamma^2(\mathbf{r})}{16}\right)^{1/2}.\end{aligned} \quad (13)$$

Here the influence of the nanoenvironment is taken into account by using effective (modified by the nanoenvironment) values for Rabi frequency and linewidths.

By taking the Fourier transform of $\langle E^{(-)}(\mathbf{r},t)E^{(+)}(\mathbf{r},t+\tau)\rangle$ with respect to τ and making use of

$$\int_0^\infty d\tau e^{-i\omega t-\gamma\tau/2+i\omega_L\tau} = \frac{1}{i(\omega-\omega_L)+\gamma/2}, \quad (14)$$

$$\int_0^\infty d\tau e^{-i\omega t\mp i\mu\tau-3\gamma\tau/4+i\omega_L\tau} = \frac{1}{i(\omega-\omega_L\pm\mu)+3\gamma/4}, \quad (15)$$

we obtain the spectral density $S(\mathbf{r},\omega_L)$ of the electromagnetic field at $\mathbf{r}$:

$$\begin{aligned}S(\mathbf{r},\omega_L) &= I_0(\mathbf{r})\sin^2\psi\left(\frac{\Omega^2(\mathbf{r})}{\gamma^2(\mathbf{r})+2\Omega^2(\mathbf{r})}\right) \\ &\quad\times\left\{\frac{\gamma^2(\mathbf{r})}{\gamma^2(\mathbf{r})+2\Omega^2(\mathbf{r})}\delta(\omega-\omega_L)+\frac{\gamma(\mathbf{r})}{(\omega-\omega_L)^2}\right. \\ &\quad\left.+\frac{\alpha_+(\mathbf{r})}{[\omega+\mu(\mathbf{r})-\omega_L]^2}+\frac{\alpha_-(\mathbf{r})}{[\omega-\mu(\mathbf{r})-\omega_L]^2}\right\},\end{aligned} \quad (16)$$

where

$$\alpha_\pm = \frac{3\gamma(\mathbf{r})}{4}P(\mathbf{r})\pm[\omega\pm\mu(\mathbf{r})-\omega_L]Q(\mathbf{r}). \quad (17)$$

From Eq. (16) one can see that the resonance fluorescence of the two-level atom in free space consists, in general, of four components, whose intensities largely depend on the intensity of the driving field and all four are of the same order of amplitude in the limit of saturating the driving atomic transition field. Decay rates in this equation define the widths of the corresponding Lorentzian lines in the spectrum, which consists of three Lorentzian profiles at the frequencies ω_L, $\omega_L \pm \Omega$ and the coherent response at the frequency ω_L [41].

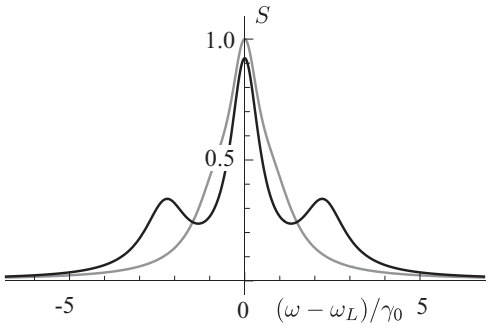

FIG. 7. The resonance fluorescence spectrum of the two-level atom with $\gamma_0 = 20$ MHz in free space (gray line) and near the nanosphere (black line) of radius $a = 20$ nm at a distance 20 nm from the nanosphere surface and $\theta = 0.3$ rad (17°), in a weak incident laser field at $\lambda = 632.8$ nm and $\Omega = 0.8\gamma_0$.

The resonance fluorescence spectra of a two-level atom in free space and near the nanosphere calculated with the help of Eqs. (4), (7)–(9), and (16) are shown in Figs. 7–9. One can clearly see that in the limit of a weak incident laser field (Fig. 7) the resonance fluorescence spectrum of the two-level atom in free space has only one pronounced line in the spectrum at the zero-frequency detuning [41]. Placing a nanobody in close proximity to the atom enhances the local field and affects the Rabi frequency and decay rate of the atom, so the spectrum of the resonance fluorescence is enriched and one can clearly see the Mollow-type triplet structure of the spectrum. Playing with these parameters opens new possibilities of controlling the properties of the atom with the help of the nanobody.

The position of the atom located in the yz plane in the vicinity of the nanosphere is characterized by two parameters:

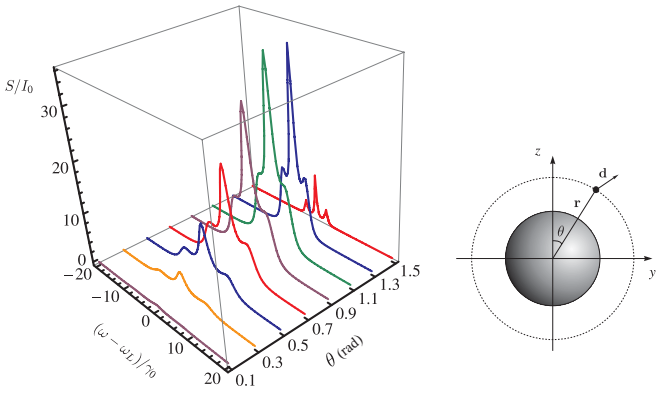

FIG. 8. (Color online) Resonance fluorescence spectrum of the two-level atom normalized to I_0 near the nanosphere of radius $a = 20$ nm vs the angle $\theta = 0.1$–1.5 rad (5.7°–85.9°). The distance of the atom from the nanosphere surface is equal to 10 nm, $\lambda = 632.8$ nm, and $\gamma_0 = 20$ MHz.

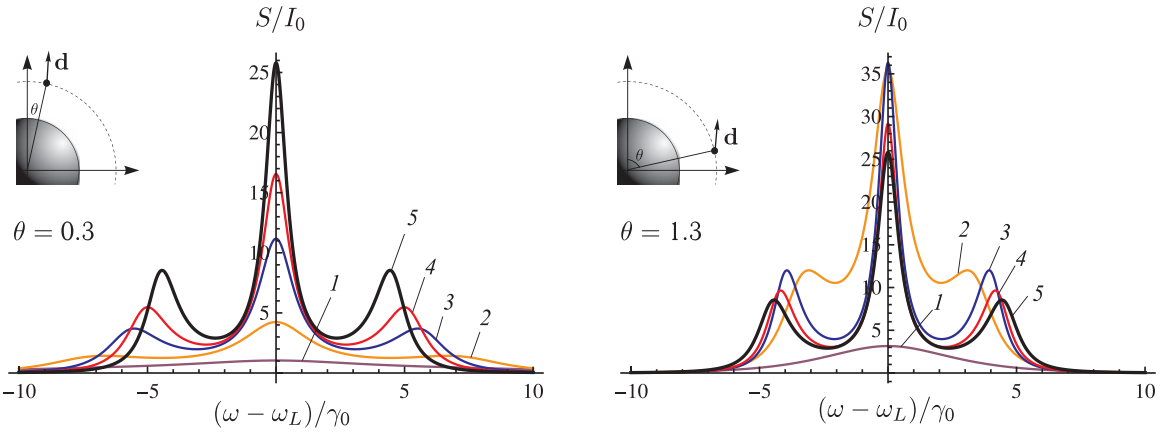

FIG. 9. (Color online) The normalized (to I_0) resonance fluorescence spectrum of the two-level atom near the nanosphere of radius $a = 20$ nm for two locations of the atom: $\theta = 0.3$ rad (17°, left) and 1.3 rad (74.5°, right). The atom-nanosphere surface distance is equal to 5 nm (violet line 1), 10 nm (orange line 2), 20 nm (blue line 3), 30 nm (red line 4), and for an atom in free space (black line 5); $\lambda = 632.8$ nm and $\gamma_0 = 20$ MHz.

the radial coordinate $|\mathbf{r}|$ and the angle θ ($\varphi = 0$). Let us fix the radial coordinate of the atom. Then, the atom is located at one of the points constituting the circle with the center coinciding with the nanosphere center. For different points of this circle, the local field intensities, the directions of the fields, as well as the atomic decay rates are different, so it is necessary to use for their calculations Eqs. (16) and (17), which correctly take into account the values of the local field modified by the nanosphere and the total atomic decay rates. In each atom's location the atomic dipole moment is codirected with the vector of the local field (see Fig. 3).

Figure 8 shows how the resonance fluorescence spectrum of the atom spaced from the surface of the nanosphere at 10 nm changes versus the angle θ of the atom's location. The resonance fluorescence spectrum depends on the position of the observer as $S \sim \sin^2\psi$ [see Eq. (16)], where ψ is the angle between the atomic dipole direction and the z axis. In our case, the observer is located at the z axis and the atomic dipole moment is codirected with the direction of the local field (see Fig. 3), so that at the angles $\theta = 0°$ (0 rad) and 90° (1.57 rad) the resonance fluorescence intensity registered by the observer from the atom in these points of space is vanishingly small. As it follows from Fig. 3, the local field intensity reaches maximum at $\theta = 0°$ and its minimum at $\theta = 90°$, so with increasing θ the satellite lines of the spectrum are shifted toward the central line due to the decreasing of the Rabi frequency. Note also that for $\theta = 1.1$ rad (67°) one can observe the maximum resonance fluorescence intensity (Fig. 8).

Let us clarify now how the resonance fluorescence spectrum of the two-level atom depends on the distance between the atom and the nanosphere surface at fixed values of angle θ (Fig. 9).

For the angle $\theta = 0.3$ rad (17°), increasing the distance between the atom and the nanosphere surface leads to a decrease of the local field at the atom location up to the value of the intensity of the incident field $\mathbf{E}_0$ and, respectively, to reducing the Rabi frequency. As a result, the satellite lines in the Mollow spectrum are shifted toward the central line. The widths of the separate lines in the spectrum are defined by the total atomic decay rate, $\gamma^{\text{total}} = \gamma^{\text{radiative}} + \gamma^{\text{nonradiative}}$. From Fig. 5 one can clearly see that at the distances 5 nm or less to the nanosphere surface the nonradiative decay rate prevails over the radiative decay rate and the fluorescence quenches (violet line 1 in Fig. 9). With increasing distance between the atom and the nanosphere surface, the nonradiative decay rate sharply vanishes as $\sim 1/|\mathbf{r}|^3$ and at the distances $\geqslant 7$ nm the radiation decay rate significantly prevails over the nonradiative one (see Fig. 5).

For the angle $\theta = 1.3$ rad (74.5°), the radial component of the local field in the atom location is almost equal to zero and the field has only a tangential component (see Fig. 3). Keeping in mind that the atomic dipole moment is codirected with the direction of the local field, one can conclude that the dipole moment is tangentially oriented toward the nanosphere. Therefore, decreasing the distance between the atom and the nanosphere surface results in narrowing the lines of the resonance fluorescence spectrum and reducing the spacing between them. At distances smaller than 5 nm, the nonradiative atomic decay rate significantly prevails over the radiative decay rate and, as a result, the fluorescence quenches (violet line 1 in Fig. 9).

In both cases considered above, the atomic dipole moment is almost codirected with the z axis, so at large distances from the atom to the nanosphere surface, i.e., when the atom is basically in free space and the influence of the nanosphere vanishes, the spectral dependencies for the angles $\theta = 0.3$ rad (17°) and $\theta = 1.3$ rad (74.5°) must coincide, which one can clearly see from Fig. 9 (black line 5).

Figure 10 presents also an analysis of how the resonance fluorescence spectrum depends on the nanosphere radius at the fixed distance between the atom and the nanosphere surface. For $\theta = 0.3$ rad (17°), the atom's dipole orientation is close to the radial one; the spectrum spreads with increasing nanosphere radius due to the increase of both the Rabi frequency and the atomic radiative decay rate. For $\theta = 1.3$ rad (74.5°), when the atom's dipole orientation is close to the tangential one, increasing the nanosphere radius leads to the

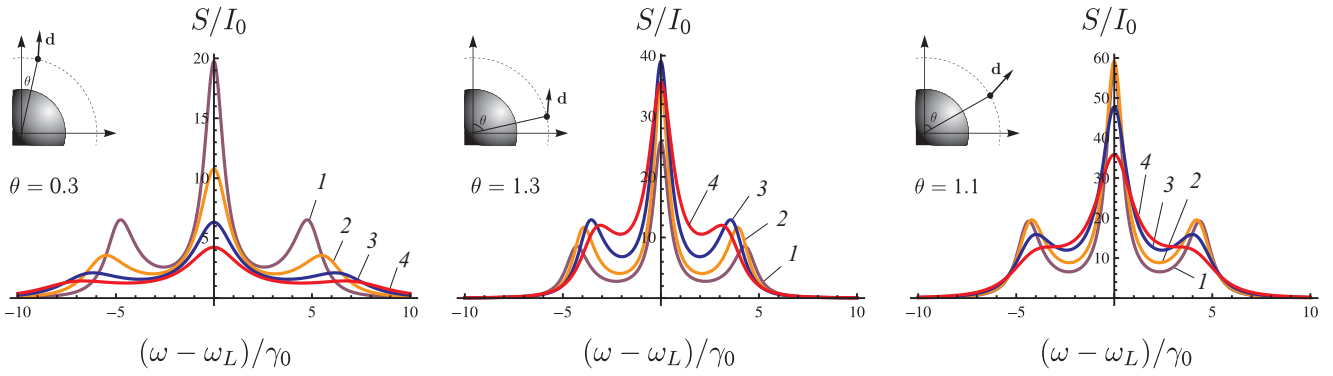

FIG. 10. (Color online) The normalized (to I_0) resonance fluorescence spectrum of the two-level atom near the nanosphere of radius $a = 5$ nm (violet line 1), 10 nm (orange line 2), 15 nm (blue line 3), and 20 nm (red line 4) for three locations of the atom with the fixed atom-nanosphere surface distance equal to 10 nm and $\theta = 0.3$ rad (17°, left), 1.3 rad (74.5°, middle), and 1.1 rad (63°, right); $\lambda = 632.8$ nm and $\gamma_0 = 20$ MHz.

decrease of the Rabi frequency and the atomic decay rate, so both the separate lines of the spectrum and the whole spectrum width become more narrow. The general tendency is that reducing the nanosphere radius leads to an increase in the contrast of the satellite lines in the spectrum.

IV. CONCLUSION

In conclusion, we have theoretically investigated modification of the resonance fluorescence spectrum of the two-level atom driven by the monochromatic field in close proximity to the plasmonic nanostructure (metal sphere). The influence of the nanoenvironment was taken into account by using effective values (modified by the nanoenvironment) for Rabi frequency and linewidths in a well-known expression for the resonance fluorescence spectrum. It is shown that one can control this spectrum varying several key parameters: (i) the radius of the nanosphere, (ii) polarization of the incident radiation, and (iii) the atom's location around the nanosphere (its radial coordinate and polar angle in a spherical coordinate system). These parameters affect the local field enhancement and the modification of the total decay rate of the atom interacting with the nanosphere, which leads to modification of the resonance fluorescence spectrum of the atom (frequency shift of the satellite lines in the Mollow-type triplet, widths of the lines, and the spectrum intensity) by contrast with the one in free space. The permittivity of the metal the nanosphere is made of is also an additional parameter that defines the nonradiative decay. In our calculations we took into account both radiative and nonradiative atomic decay rates. It is shown that at distances to the surface of the nanosphere shorter than 5 nm one can observe quenching of fluorescence, which is revealed in the drastic widening of the spectral components and sharp vanishing of the fluorescence intensity. Therefore, by varying the parameters of this nonradiative decay one can continuously control the transition from resonance fluorescence enhancement to its quenching.

In this paper, we consider the simplest case of the plasmonic nanostructure, the metal nanosphere, which allows simple analytical calculations. More complex nanostructures, however, allow more complex distribution of the local field near the nanostructure (see, for instance, Refs. [39,52]) and therefore many more degrees of freedom to control the optical properties of the emitter (atom, molecule, quantum dot, etc.) and the resulting fluorescence. In addition, multilevel quantum emitters, the simplest case of which is a three-level atom, display a much broader range of quantum effects as a result of coherence among the states induced by the incident radiation and quantum interference. They offer the whole new spectrum of possibilities for quantum control of the emitter via parameters of the nanoparticle and the incident field.

Note also that in experiments that employ the fluorescence studies of single emitters near the nanoparticle the latter is frequently surrounded or even covered by a number of these emitters [3]. In this case, to simulate the fluorescence it is necessary to take into account that the fluorescence drastically depends on the position of each emitter and on the position relative to the observer and the nanoparticles and to average over all possible values in the specific experimental setting distances and orientations. Cooperative effects in resonance fluorescence also come into the play here and must be taken into account [53].

Finally, a detailed understanding of a single quantum emitter fluorescence, including the resonance fluorescence, modified by a plasmonic nanoparticle located in close proximity is extremely important for the development of nanoscale sensors and biosensing [54,55], for the whole field of nanoplasmonics [3,56], and in surface-enhanced microscopy and spectroscopy [57–60]. Moreover, the resonance fluorescence at the nanoscale opens new horizons in studying quantum-optical effects at this scale.

ACKNOWLEDGMENTS

V.K. would like to thank the Russian Foundation for Basic Research (Grants No. 11-02-91065, No. 11-02-92002, No. 11-02-01272, No. 12-02-90014, and No. 12-02-90417) and the Presidium of the Russian Academy of Sciences for partial financial support.

[1] A. Sommerfeld, Ann. Phys. (Leipzig) **28**, 665 (1909).
[2] E. M. Purcell, Phys. Rev. **69**, 681 (1946).
[3] V. V. Klimov, *Nanoplasmonics: Fundamentals and Applications* (Pan Stanford, Singapore, 2012).
[4] V. V. Klimov, M. Ducloy, and V. S. Letokhov, Sov. J. Quantum Electron. **31**, 569 (2001).
[5] A. Salomon, C. Genet, and T. W. Ebbesen, Angew. Chem. **121**, 8904 (2009).
[6] V. V. Klimov, V. S. Letokhov, and M. Ducloy, Laser Phys. **17**, 912 (2007).
[7] V. V. Klimov, M. Ducloy, and V. S. Letokhov, Phys. Rev. A **59**, 2996 (1999).
[8] R. R. Chance, A. Prock, and R. Silbey, Adv. Chem. Phys. **37**, 1 (1978).
[9] R. X. Bian, R. C. Dunn, X. S. Xie, and P. T. Leung, Phys. Rev. Lett. **75**, 4772 (1995).
[10] L. Novotny, Appl. Phys. Lett. **69**, 3806 (1996).
[11] M. Thomas, J.-J. Greffet, R. Carminati, and J. R. Arias-Gonzales, Appl. Phys. Lett. **85**, 3863 (2004).
[12] R. Carminati, J.-J. Greffet, C. Henkel, and J. M. Vigoureux, Opt. Commun. **261**, 368 (2006).
[13] J. N. Farahani, D. W. Pohl, H.-J. Eisler, and B. Hecht, Phys. Rev. Lett. **95**, 017402 (2005).
[14] B. C. Buchler, T. Kalkbrenner, C. Hettich, and V. Sandoghdar, Phys. Rev. Lett. **95**, 063003 (2005).
[15] K. L. Kelly, E. Coronado, L. L. Zhao, and G. C. Schatz, J. Phys. Chem. B **107**, 668 (2003).
[16] J. B. Jackson and N. J. Halas, Proc. Natl. Acad. Sci. USA **101**, 17930 (2004).
[17] C. E. Talley, J. B. Jackson, C. Oubre, N. K. Grady, C. W. Hollars, S. M. Lane, T. R. Huser, P. Nordkander, and N. J. Halas, Nano Lett. **5**, 1569 (2005).
[18] H. Wei, F. Hao, Y. Huang, W. Wang, P. Nordlander, and H. Xu, Nano Lett. **8**, 2497 (2008).
[19] J. F. Li *et al*., Nature (London) **464**, 392 (2010).
[20] S. Nie and S. R. Emory, Science **275**, 1102 (1997).
[21] S. Nie and R. N. Zare, Annu. Rev. Biophys. Biomol. Struct. **26**, 567 (1997).
[22] K. Kneipp, Y. Wang, H. Kneipp, L. T. Perelman, I. Itzkan, R. R. Dasari, and M. S. Feld, Phys. Rev. Lett. **78**, 1667 (1997).
[23] X. S. Xie and J. K. Trautman, Annu. Rev. Phys. Chem. **49**, 441 (1998).
[24] K. Kneipp, H. Kneipp, I. Itzkan, R. R. Dasari, and M. S. Feld, Chem. Rev. **99**, 2957 (1999).
[25] J. Jiang, K. Bosnick, M. Maillard, and L. Brus, J. Phys. Chem. B **107**, 9964 (2003).
[26] J. A. Dieringer, R. B. Lettan II, Karl A. Scheidt, and R. P. Van Duyne, J. Am. Chem. Soc. **129**, 16249 (2007).
[27] S. Kühn, G. Mori, M. Aglio, and V. Sanddoghdar, Mol. Phys. **106**, 893 (2008).
[28] K. T. Shimizu, W. K. Woo, B. R. Fisher, H. J. Eisler, and M. G. Bawendi, Phys. Rev. Lett. **89**, 117401 (2002).
[29] A. Kramer, w. Trabesinger, B. Hecht, and U. P. Wild, Appl. Phys. Lett. **80**, 1652 (2002).
[30] E. Dulkeith, M. Ringler, T. A. Klar, J. Feldmann, A. M. Javier, and W. J. Parak, Nano Lett. **5**, 585 (2005).
[31] W. Trabesinger, A. Kramer, M. Kreiter, B. Hecht, and U. P. Wild, Appl. Phys. Lett. **81**, 2118 (2002).
[32] J. T. Krug II, E. J. Sanchez, and X. S. Xie, Appl. Phys. Lett. **86**, 233102 (2005).
[33] M. Sukharev and T. Seideman, J. Phys. Chem. A **113**, 7508 (2009).
[34] H. G. Frey, S. Witt, K. Felderer, and R. Guckenberger, Phys. Rev. Lett. **93**, 200801 (2004).
[35] V. V. Klimov, M. Ducloy, and V. S. Letokhov, J. Mod. Opt. **43**, 2251 (1996).
[36] A. Kinkhabwala *et al*., Nat. Photonics **3**, 654 (2009).
[37] P. Anger, P. Bharadwaj, and L. Novotny, Phys. Rev. Lett. **96**, 113002 (2006).
[38] S. Kühn, U. Hakanson, L. Rogobete, and V. Sandoghdar, Phys. Rev. Lett. **97**, 017402 (2006).
[39] Y. Gu, L. Huang, O. J. F. Martin, and Q. Gong, Phys. Rev. B **81**, 193103 (2010).
[40] O. Astafiev, A. M. Zagoskin, A. A. Abdumalikov, Yu. A. Pashkin, T. Yamamoto, K. Inomata, Y. Nakamura, and J. S. Tsai, Science **327**, 840 (2010).
[41] H. J. Kimble and L. Mandel, Phys. Rev. A **13**, 2123 (1976).
[42] G. Slavcheva, J. M. Arnold, I. Wallace, and R. W. Ziolkowski, Phys. Rev. A **66**, 063418 (2002).
[43] M. Sukharev and A. Nitzan, Phys. Rev. A **84**, 043802 (2011).
[44] A. Fratalocchi, C. Conti, and G. Ruocco, Phys. Rev. A **78**, 013806 (2008).
[45] Such plasmonic nanostructures are technologically made of gold or silver, which are standard materials for optical nanoantennas as they have relatively low losses in the optical range of frequencies.
[46] This is not correct for the molecules that would have a permanent dipole moment in the ground state. In this case, the total dipole moment of the molecule will be composed of the permanent dipole moment in the ground state and that induced in the excited state. The induced dipole moment will be codirected in the direction of the local field, whereas the permanent dipole moment will keep its initial direction.
[47] P. A. Apanasevich, Opt. Spectrosc. **14**, 612 (1963).
[48] P. A. Apanasevich, Opt. Spectrosc. **16**, 709 (1964).
[49] M. Newstein, Phys. Rev. **167**, 89 (1968).
[50] B. R. Mollow, Phys. Rev. **178**, 1969 (1969).
[51] H. Walther, Adv. At. Mol. Opt. Phys. **51**, 239 (2005).
[52] A. M. Kern and O. J. F. Martin, Nano Lett. **11**, 482 (2011).
[53] S. J. Kilin, J. Phys. B **13**, 2653 (1980).
[54] J. N. Anker, W. P. Hall, O. Lyandres, N. C. Shah, J. Zhao, and R. P. van Duyne, Nat. Mater. **7**, 442 (2008).
[55] T. Sannomiya and J. Vörös, Trends Biotechnol. **29**, 343 (2011).
[56] L. Novotny and N. van Hulst, Nat. Photonics **5**, 83 (2011).
[57] S. M. Flores and J. L. Toca-Herrera, Nanoscale **1**, 40 (2009).
[58] F. J. Garcia de Abajo, Rev. Mod. Phys. **82**, 209 (2010).
[59] A. P. D. Elfick, A. R. Downes, and R. Mouras, Anal. Bioanal. Chem. **396**, 45 (2010).
[60] B. Pettinger, Mol. Phys. **108**, 2039 (2010).